Multifractal analysis of tensile toughness and filler dispersion for polypropylene–CaCO$_3$ composites

E. Pérez [a,*], C. Bernal [a], M. Piacquadio [b]

[a] *Advanced Materials Group, INTECIN (UBA-CONICET), Department of Mechanical Engineering, Engineering Faculty, University of Buenos Aires, Av. Paseo Colón 850, C1063ACV, Buenos Aires, Argentina*
[b] *Secretary of Investigation and Doctorate, Engineering Faculty, University of Buenos Aires, Av. Paseo Colón 850, C1063ACV, Buenos Aires, Argentina*

ARTICLE INFO

ABSTRACT

Multifractal analyses were performed to elucidate the effect of incorporating maleic anhydride grafted polypropylene (MAPP) into a Polypropylene matrix: (i) on the dispersion of CaCO$_3$ particles and (ii) on the fracture morphology of tensile samples. The box-counting method was applied considering the number of particles and the mean gray value distribution as measured properties of composites. The dispersion analysis exhibited, for the composite with MAPP, a reduction of larger agglomerates sizes without variation of the most frequent size. Similar results were achieved by a typical particle size distribution. Moreover, the morphology of fractured surfaces showed an irregular topography for composites without MAPP suggesting a complex fracture process. Composites with MAPP, on the contrary, displayed a regular surface morphology suggesting a more regular fracture process with an important reduction of ductile mechanisms. This fracture behavior was related to the variation of the singularity width $\Delta\alpha$. The results obtained suggest that multifractal theory can be applied to elucidate the relationship between structure and mechanical behavior of PP–CaCO$_3$ composite materials.

1. Introduction

Polypropylene (PP), its blends and composites are extensively used in home, electronic, automobile, packaging and construction, among other appliances [1,2]. However, the use of PP as a structural material is still limited due to its relatively poor toughness at low temperature and high strain rates, especially in the presence of notches [3]. In order to induce enhancements in mechanical properties such as stiffness, strength, fracture resistance, impact toughness, wear resistance, hardness, etc. inorganic rigid particles are usually incorporated into PP [3–5]. In addition, the mechanical properties of composites are related to the dispersion, type, size and shape, content and surface treatment of the fillers [6]. These fillers tend to form agglomerates, increasing with decreased particle size and increased filler content which are detrimental to the material mechanical behavior. To bring the effect of the particles into play, agglomerates should be broken during mixing processes [7]. Uniform dispersion of the filler in the polymer matrix avoids the creation of crack-initiating large agglomerates [8].

Dispersion and interfacial adhesion of the fillers have been successfully improved by using polymeric coupling agents such as grafted polyolefins [4,9,10]. For example, PP grafted with maleic anhydride (MAPP) is extensively used in PP-based composites [4,10]. However, it should be pointed out that, coupling agents can introduce simultaneously both detrimental and beneficial effects. The balance of these counteracting effects defines the final properties of the composites.

In order to study particle dispersion and matrix-filler interaction different experimental as well as theoretical methods are usually applied. Rheological measurements, Cole-Cole diagrams, dynamic mechanical analysis, morphological observations, particle size distribution analysis, fractal theory, analytical solutions and finite elements analysis, among others have been successfully used [5,9–13].

The complex morphology of fracture surfaces can be analyzed to describe fracture behavior and to elucidate the presence of different fracture processes. In general, a rough surface is related to a ductile fracture while a flat surface to a brittle one [14]. A quantitative description of the complex morphology of fracture surfaces has been already successfully analyzed by multifractal theory in the case of different materials [15,16].

Many different methods, algorithms, formalisms, and spectra, have been developed to display data connected with fractal phenomena [16–20]. Some of them are briefly discussed on Section 2.4, but an extensively review is entirely beyond the scope of this paper.

In this work, the dispersion of CaCO$_3$ microparticles and the morphology of fracture surfaces of PP-based composites were analyzed by the multifractal theory. Characteristic parameters of

* Corresponding author.
 E-mail address: emperez05@hotmail.com (E. Pérez).

the multifractal spectra were used to estimate the relationship between particle dispersion, surface morphology of tested samples and tensile behavior of the composites. The accuracy of the experimental procedure used to calculate multifractal spectra was also discussed.

2. Material and methods

2.1. Preparation of composite materials

A commercial polypropylene (PP) (CUYOLEN 1100N) kindly provided by Petroquímica Cuyo, Mendoza, Argentina, with a melt flow index of 11 g/10 min and a density of 0.9 g/ml was used as the matrix of the composites. Filler was calcium carbonate (CaCO$_3$) microparticles with content of 20 wt.% provided by Sigma–Aldrich. The components were mixed in an intensive mixer at 190 °C and 50 r.p.m for 10 min. Then, composite sheets (nominal thickness B = 0.5 mm) were compression molded in a hydraulic press at 180 °C under a pressure of 100 kPa for 10 min. Finally, the sheets were rapidly cooled by circulating water within the press plates under a pressure of 100 kPa. In order to improve the dispersion of the filler in the PP matrix, composites with 10 wt.% of maleic anhydride grafted PP (MAPP) (Epolene E-43 wax, Eastman Chemical Company, USA) were also prepared in a similar manner.

2.2. Mechanical tests and morphological observations

Uniaxial tensile tests were carried out in a universal testing machine (Interactive Instruments 10 K) at a crosshead speed of 5 mm/min for the composite materials in accordance with ASTM D882-02 standard recommendations. Tensile parameters values were originally reported in Ref. [21]. Fracture surfaces of specimens broken in tensile tests were analyzed by scanning electron microscopy (SEM) after they had been coated with a thin layer of gold. Images from different samples of both composite materials were obtained with magnifications of 500× and 1010×.

2.3. Particle size distribution

Filler size and cumulative size distributions were obtained from SEM micrographs of fracture surfaces. Quantitative image analysis was performed with the help of the image processing software Image J. In order to warrant statistical validity of the image analysis, a minimum of 300 particles were measured. Cumulative size distributions were determined by summing the fractions of particles that are smaller than a specific size.

2.4. Multifractal analysis and experimental application

The theory of multifractal spectra called *fine* and *coarse*, stems from the Hausdorff dimension and the Kolmogorov–Minkowski dimension, called dim$_H$ and dim$_B$, respectively [22]. The *coarse* dimension stems from the *fine* one by crossing out one condition in the definition of dim$_H$: the two spectra are thus conceptually linked, and naturally associated. The Kolmogorov–Minkowski dimension, dim$_B$, is the adaptation of dim$_H$ to solve problems in physics and other applied sciences. The problem with the more *fine* dim$_H$ is that it is =(identically equal to) zero, for any finite set of elements, or even a numerable infinity of them.

In the present work, limited experimental data are analyzed and we wish to be careful in our choice of fractal dimension. It was considered the Kolmogorov–Minkowski dimension definition (dim$_B$) for it stems directly from Hausdorff's (par excellence *the mathematical tool* defining the concept of dimension).

In the last few years many multifractal formalisms have been proposed, using different concepts of dimension applied to objects and phenomena of a fractal nature. For each such concept of dimension (packing, compass, Legendre, thermodynamical, Renyi––maximum or minimum, etc.) there is a corresponding spectrum or formalism. For example: the thermodynamic algorithms, or the partition function method, two-dimensional multifractal detrending moving average analysis (2D MF-DMA), cross-correlation method, the two-dimensional multifractal detrended fluctuation analysis (2D MF-DFA) among others [16–19].

It should be pointed out that, some of these methods are not sensitive enough to obtain the whole information of the system under study due to some imposed spectral characteristics. For example, the thermodynamic algorithms, or the partition function method imposes continuity of $f(\alpha)$, smoothness, negative second order derivative, tangency to the bisectriz of the first quadrant. For instance, the Renyi spectrum, generalizing the entropy dimension, can be non-differentiable and even discontinuous (which permits detecting, e.g., different types of phase transitions) [15,16,22,23].

On the contrary, *spectra by definition* represent a more sensitive method capable to detect discontinuities of the corresponding ($f(\alpha)$ vs. α) curves. This occurs when different physical phenomena are simultaneously present and there is more than one fractal measure involved [24–27]. If there is only one underlying measure involved, the corresponding spectrum by definition would be continuous, smooth, and could partake of several characteristics of the thermodynamical one.

Dispersion of the filler into the PP matrix and morphology of fractured surfaces were analyzed by the box counting method applied on SEM images of both magnifications. The images were covered with a grid of boxes length ε = 1/2, 1/4, 1/6, 1/11, 1/12, 1/13 and 1/25. Multifractal spectra were calculated based on a defined measure as follow:

$$\mu_{ij}(\varepsilon) = \frac{n_{ij}}{\sum n_{ij}}$$

where $\mu_{ij}(\varepsilon)$ represent the number of particles probability in the box (i,j), n_{ij} is the number of particles contained in the box (i,j) of size ε. The defined measure $\mu_{ij}(\varepsilon)$ can be decomposed in a multifractal spectrum $(\alpha, f(\alpha))$ defining α and $f(\alpha)$ by:

$$\mu_{ij}(\varepsilon) \propto \varepsilon^{\alpha}$$

$$N_{\alpha}(\varepsilon) \propto \varepsilon^{-f(\alpha)}$$

where N_{α} is the number of boxes with the same value of α.

Let us recall, that the α-concentration of a box is the log/log version of the density, of mass or measure per unit of length:

$$\alpha(\varepsilon) = \frac{\log(\mu_{ij}(\varepsilon))}{\log(\varepsilon)}$$

The spectrum $f(\alpha)$ represents the fractal dimension of the α-concentration subset:

$$f(\alpha) = \frac{\log(N_{\alpha})}{\log(\varepsilon)}$$

and will be called *spectrum by definition*.

It should be pointed out, since $\varepsilon < 1$, that the α_{min} value is related to the larger agglomerates probability and the α_{max} value to the smaller agglomerates, perhaps isolated particles. Parameter $\Delta\alpha = (\alpha_{max} - \alpha_{min})$ describes the range of probabilities; a larger value corresponds to a wider probability distribution [16]. The $f(\alpha)$ values are related to the number of boxes with the same size agglomerates probability. Moreover, the parameter $\Delta f(\alpha) = (f(\alpha_{min}) - f(\alpha_{max}))$ indicates the difference on the fractal dimension corresponding to the maximum and minimum of the spectra.
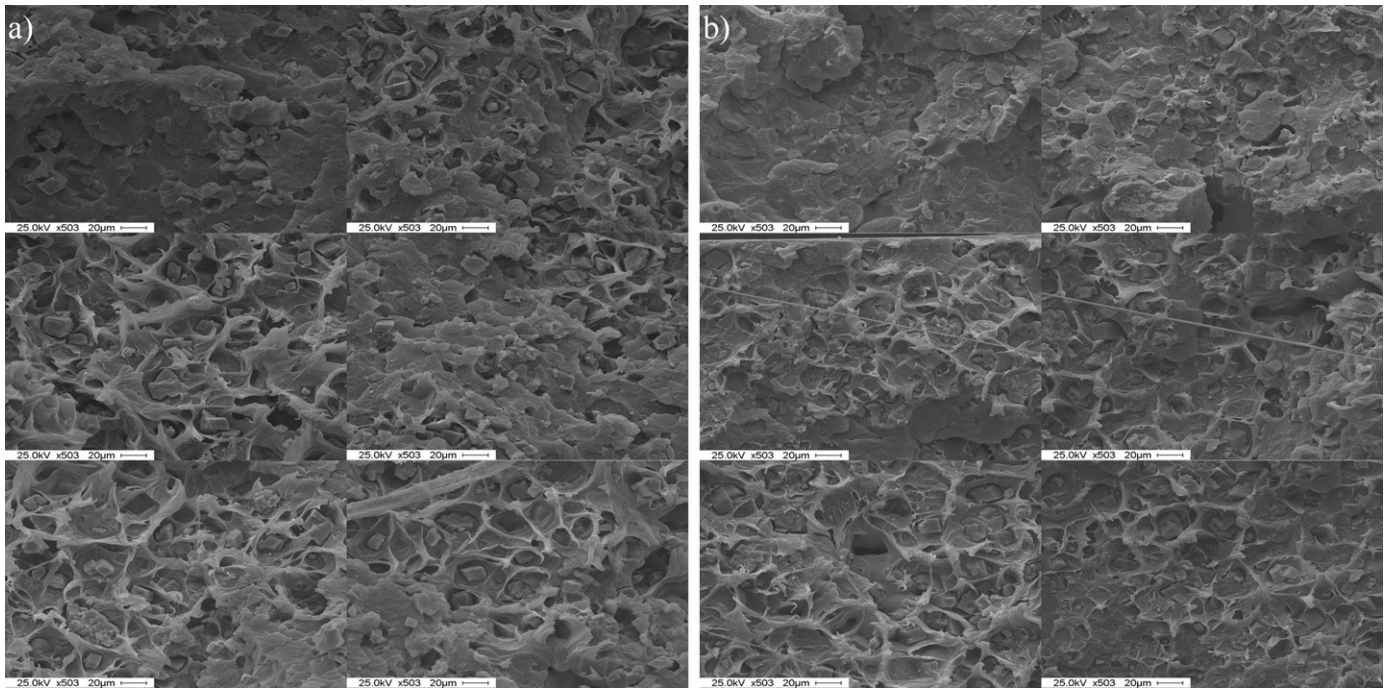
Fig. 1. SEM micrographs (500×) of fractured surfaces: (a) PP–20 wt.% CaCO$_3$ and (b) PP–10 wt.% MAPP–20 wt.% CaCO$_3$.

In a similar way the multifractal spectra to analyze the complex morphology of fractured surfaces was determined. The defined measure ($\mu_{ij}(\varepsilon)$) considered was the mean gray value distribution probability. In this case, α_{min} is related to the maximum gray value distribution probabilities and α_{max} to the minimum ones.

Finally, for experimental multifractal decomposition some practical limitations appear. For example, an infinity of elements are theoretically required, clearly an impossibility in an experimental situation. As pointed out above, both α and $f(\alpha)$ are calculated by *definition* throughout this work.

3. Results and discussion

3.1. Dispersion of the CaCO$_3$ filler in the PP matrix

Fig. 1a and b shows SEM micrographs of fracture surfaces of PP-based composites without and with MAPP, respectively. Qualitatively, CaCO$_3$ particles and its agglomerates are uniformly distributed in the matrix independently of the presence of the coupling agent. Therefore, the incorporation of MAPP in the composite formulation does not induce any obvious change in the dispersion of the particles.

3.2. Multifractal analysis of filler dispersion in the PP matrix

The multifractal analysis was performed applying the box counting method as following: Firstly, a global image of each system was obtained considering the different SEM micrographs. In each global image the presence of particles were identified with a number as shown in Fig. 2. After identification, the global image was covered with a grid of many boxes of size $\varepsilon \times \varepsilon$ and counted the particle quantity inside of every box. The obtained values of $\mu_{ij}(\varepsilon)$ and $N(\alpha)$ were also used to calculated the corresponding multifractal spectra.

An ideal regular multifractal exhibits a straight line in the log $N(\varepsilon)$ vs. log ε graph over the scaling range. However, in spatial fractals the scaling range is generally reduced due to the properties of the measured system or limitations of the apparatus considered.

Moreover, scaling range can be deformed by high-order trends or nonlinearity [28]. For agglomeration experiments, the empirically measured scaling range was reported close to one order of magnitude [29]. Fig. 3 shows a linear regression for the PP–20%CaCO$_3$ composite in the range from $\varepsilon = 1/2$ to 1/25, close to one order of magnitude. This result suggests that, it is possible to describe the dispersion of the fillers quantitatively by the multifractal theory. The log $N(\varepsilon)$ vs. log ε plot for the other composite material was obtained by the same method (not shown here).

Multifractal *spectra by definition* ($f(\alpha)$ vs. α) based on SEM micrographs with a magnification of 500× and 1010× are presented in Fig. 4a and b, respectively. Fig. 4a displays increased α_{min} and α_{max} values, while the most frequent α value ($\alpha(f_{max})$) was not affected by the incorporation of MAPP in the composite formulation. Decreased values of $f(\alpha)$ were achieved in the range from α_{min} to $\alpha(f_{max})$, especially the most important reduction was placed at $\alpha(f_{max})$. On the contrary, increased $f(\alpha)$ values were obtained in the range from $\alpha(f_{max})$ to α_{max}.
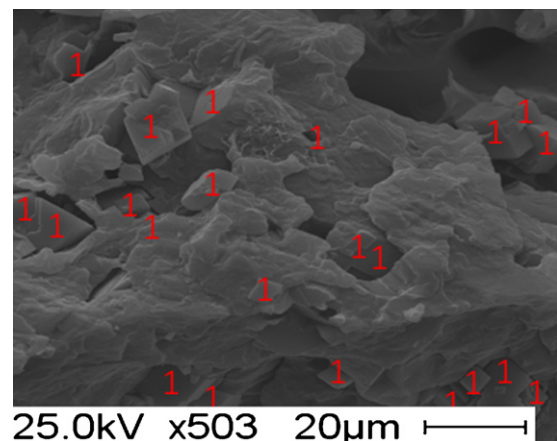
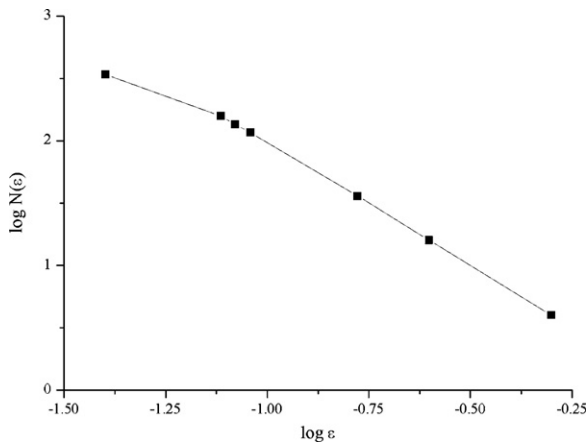**Fig. 2.** Partial amplification of Fig. 1a with identification of the particles.

Fig. 3. log $N(\varepsilon)$ vs. log ε plot for fillers dispersion analysis.

Fig. 5. Histogram and cumulative of particle size distribution for the CaCO$_3$ obtained from SEM micrographs.

Closer views of the particles within the PP matrix were investigated to analyze the effect of MAPP on the dispersion of the filler. Calculated curves based on SEM micrographs, with a magnification of 1010× are plotted in Fig. 4b. The spectra exhibit a multifractal behavior for smaller α value, while a dispersive zone is detected close to α_{max}, especially in the absence of the coupling agent. It means that in the composite material, these α-concentration subsets are not related to a multifractal behavior. The composite with coupling agent incorporates the isolated particles and smaller agglomerates into the multifractal features established by the particles into the PP matrix. This probable effect was not detected with a smaller magnification (500×).

Smooth curves calculated with the smaller magnification strictly correspond to multifractal spectra without dispersive behavior. Quantification of the effect of MAPP on the dispersion of CaCO$_3$ particles was based on these results. Table 1 lists the characteristic parameters of the multifractal analysis.

Multifractal spectra were determined from different SEM magnifications and box sizes to discuss the accuracy of the experimental procedure used. The results obtained display their best relation to multifractal spectra (*smooth curves*) for SEM micrographs with a magnification of 500×. It is possible to relate instability of the curves to the number of the particles analyzed, considered as deviating factor for experimental results respect to theoretical predictions.

The results discussed above suggest that the incorporation of MAPP had the following effects: (i) for the largest agglomerates a reduction of its size and frequency probability, (ii) a reduction on the frequency of the most frequent agglomerate size probability without a reduction of their size probability, and (iii) a reduction of the size of smallest agglomerates, or isolated particles, probability.
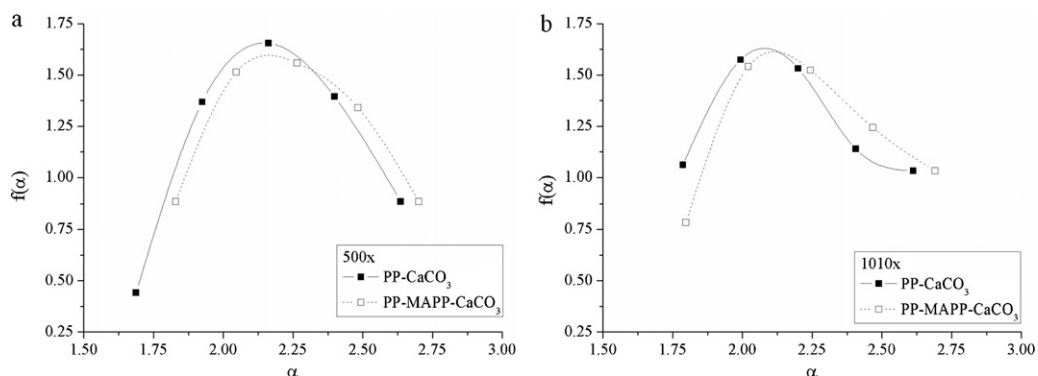
It is possible to consider the most frequent agglomerate size probability as an intrinsic property of the PP-based composites analyzed, not affected by the coupling agent.

3.3. Particle size distributions

SEM micrographs were used to obtain particle size distributions within the PP matrix. It can be observed in Fig. 5 that, the curve for the PP–20 wt.% CaCO$_3$ composite has an irregular particle size distribution with a shoulder close to the most frequent particle size and a tail at larger particle sizes, probably related to the presence of agglomeration [5]. The composite with coupling agent presents a slight shift of the distribution toward smaller particle sizes, without any shoulder and with a smaller tail at larger particles sizes. Median values were 9.45 μm and 8.12 μm for composites without and with MAPP, respectively. The cumulative curve for the PP–10 wt.% MAPP–20 wt.%CaCO$_3$ composite exhibits an increased contribution of smaller particle sizes.

The above results indicate that the composite with MAPP, presents a reduction in the frequency and size of larger agglomerates increasing the frequency of smaller agglomerates and dispersed particles. Similar results were found using multifractal analysis.

3.4. Multifractal analysis of fracture surfaces

In order to analyze the complex morphology of the fractured surfaces, the mean gray value distribution was considered. A similar procedure, as described on Section 3.2, was applied. The SEM

Fig. 4. Multifractal spectra for the CaCO$_3$ particles dispersion based on SEM micrographs: (a) 500× and (b) 1010× magnification.
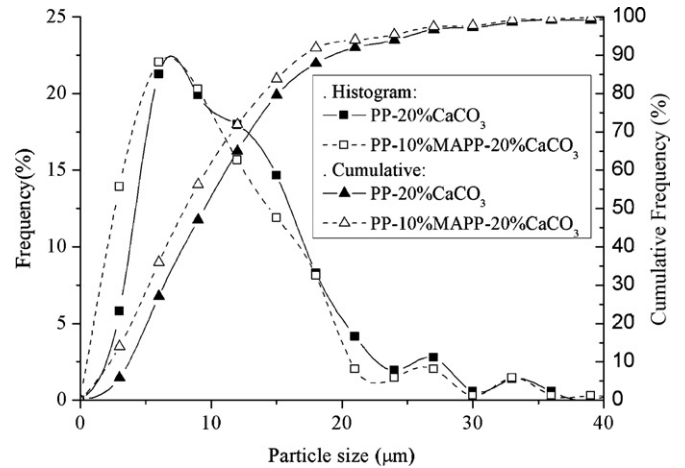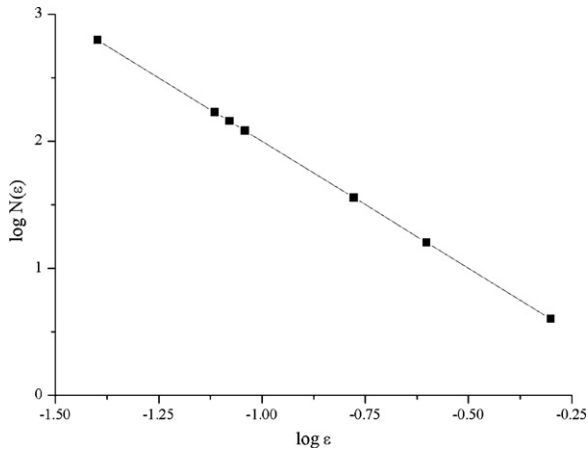
Table 1
Multifractal spectra parameters for the PP-based composites investigated.

	α_{min}	α_{max}	$\Delta\alpha$	$f(\alpha_{min})$	$f(\alpha_{max})$	$\Delta f(\alpha)$
PP–20%CaCO$_3$	1.68783	2.63577	0.94794	0.44211	0.88423	−0.44212
PP–10%MAPP–20%CaCO$_3$	1.82916	2.70100	0.87184	0.88423	0.88423	−0.0001

Fig. 6. $\log N(\varepsilon)$ vs. $\log \varepsilon$ plot for morphology of fractured surfaces analysis.

Fig. 8. Variation of the singularity width $\Delta\alpha$ for fillers dispersion and morphology of fractured surfaces with truncated data.
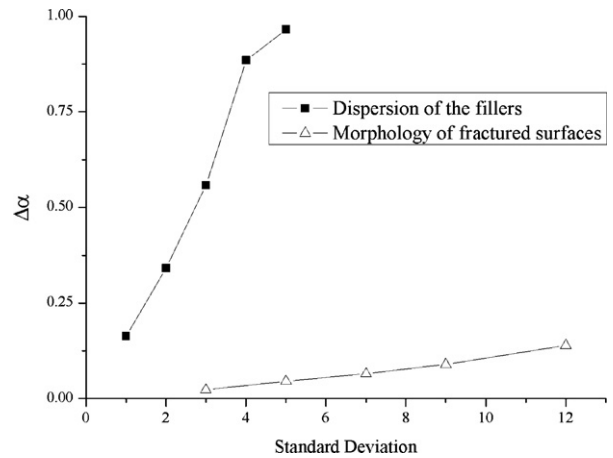
micrographs were reduced to eliminate the noises introduced by the marks on the images. The values of every box were obtained by the function: analyze/measure of the ImageJ software. As a linear relationship is observed in Fig. 6, the multifractal theory can be applied to study the topography of fractured surfaces. Similar scaling ranges were reported on the literature [29].

In Fig. 7 for the composite without MAPP a wider $\Delta\alpha$ (reduced α_{min} and larger α_{max} values) was observed. It has been established in the literature that a wider $\Delta\alpha$ suggests a more irregular and complex fracture surface [15,16,30]. Moreover, the α_{max} and α_{min} values can be related to ductile and brittle fracture mechanisms, respectively [15,16]. On the contrary, the spectrum for the composite with MAPP suggests a more regular fracture process with an important reduction of ductile mechanisms.

With regards to the toughening mechanisms, debonding of the particles is recognized as a ductile one that can induce ductile tearing of the PP matrix and is detected by a rougher surface [14]. This behavior was clearly observed in the SEM fractographs for the composite without MAPP, in correspondence to a relatively ductile fracture.

Fig. 7. Multifractal spectra for the fractured surfaces of the PP-based composites investigated.

The characteristic parameters of the spectra listed in Table 2 are related to the simultaneous action of brittle and ductile mechanisms which determines the whole fracture behavior of the samples.

3.5. Mechanical properties and multifractal relationship

The importance of analyzing the dispersion of the particles and the morphology of the fracture surfaces lays on their close relationship with the mechanical behavior of composite materials. Moreover, in this section we try to elucidate the possible origins of multifractality and its correlation with the materials mechanical properties. This analysis can be done by statistical methods, such as: linear long-range correlations, long-tails of the distribution, nonlinear correlations, among others [28,31,32].

The extreme values should be progressively eliminated (the truncation method) to understand their impact on the singularity width $\Delta\alpha$ [28]. Fig. 8 shows (for dispersion of the fillers in the PP–20%CaCO$_3$ composite) that, when the values were progressively truncated the singularity width $\Delta\alpha$ decrease dramatically. The corresponding curve, for fractured surfaces analyses, display a slightly decrease on the singularity width $\Delta\alpha$. These results indicate that, the extreme values have significant effect on the multifractality (especially in the case of dispersion of the fillers).

A first approach to elucidate the origin of multifractality can be: (i) for dispersion of the fillers, due to the presence of the largest agglomerates sizes (on one side) and isolated particles (on the other side), (ii) for morphology of the fractured surfaces, possibly, due to ductile tearing of the matrix after debonding of the particles (on one side) and to the brittle fracture of the PP matrix (on the other side).

More calculations are required, but it is not possible to perform an extensively study of this important point based on the limitation of the data analyzed. Some statistical and detailed investigation will be considered in further works.

Finally, the dispersion of the particles was considered in a previous work by a theoretical model predicting the tensile strength of the composites [21]. In this simple model, deviation from a linear fitting means the appearance of some structural effect.

Table 2
Multifractal spectra parameters for the gray scale values for the PP-based composites.

	α_{min}	α_{max}	$\Delta\alpha$	$f(\alpha_{min})$	$f(\alpha_{max})$	$\Delta f(\alpha)$	Tensile toughness (J/m)
PP–20%CaCO$_3$	1.88495	2.12019	0.23524	1.35119	0.75865	0.59254	1.3 ± 0.3
PP–10%MAPP–20%CaCO$_3$	1.88495	2.04168	0.15673	1.35119	0.54048	0.81071	0.8 ± 0.1

For our PP–20 wt.% CaCO$_3$ composite experimental data of tensile strength vs. filler volume fraction deviated from a linear fit whereas composites with MAPP shift deviation to higher particle content (30 wt.% CaCO$_3$) [21]. This observation suggests that, MAPP promoted a better dispersion of the CaCO$_3$ particles detected by the model (linear fitting) and by multifractal spectra analysis (larger α values).

Although the addition of MAPP can induce an enhancement in the dispersion of the particles into PP, it was detrimental for the composites tensile behavior [21]. Decreased tensile toughness was found for the composite with MAPP. Moreover, multifractal analysis showed a decreased $\Delta\alpha$ value corresponding to decreased tensile toughness for the investigated composite materials. Similar results were reported in the literature for polyvinylidene chloride/glass fiber composites [15].

4. Conclusions

The relationship among dispersion of CaCO$_3$ particles, morphology of fracture surfaces and composites tensile behavior was investigated by multifractal theory.

From the application of multifractal theory, it was found that the incorporation of MAPP led to an improvement in the dispersion of the particles in the PP matrix. This behavior was detected by multifractal theory and particle size distribution, suggesting the accuracy of the experimental procedure applied.

In addition, multifractal analysis applied to fracture surfaces morphology showed that a wider spectrum existed for the composite without MAPP. This observation was related to a more irregular and complex fracture mechanism. Composites with MAPP displayed reduced $\Delta\alpha$ values related to brittle fracture processes. Both results were in agreement with the results of tensile tests and the qualitative morphological observations of fracture surfaces.

From the results obtained in this investigation, it can be concluded that experimental multifractal analysis based on SEM micrographs represents a powerful tool to investigate the mechanical behavior of composite materials.

References

[1] C.O. Rohlmann, M.D. Failla, L.M. Quinzani, Linear viscoelasticity and structure of polypropylene–montorillonite nanocomposites, Polymer 47 (2006) 7795–7804.
[2] Q.X. Zhang, Z.Z. Yu, X.L. Xie, Y.W. Mai, Cristallization and impact energy of polypropylene/CaCO$_3$ nanocomposites with nonionic modifer, Polymer 45 (2004) 5985–5994.
[3] A.S. Argon, R.E. Cohen, Toughenability of polymers, Polymer 44 (2003) 6013–6032.
[4] S.-Y. Fu, X.-Q. Feng, B. Lauke, Y.-W. Mai, Effects of particle, size, particle/matrix adhesion and particle loading on mechanical properties of particulate-polymer composites, Composites Part B Engineering 39 (2008) 933–961.
[5] A. Kiss, E. Fekete, B. Pukánszky, Aggregation of CaCO$_3$ particles in PP composites: effect of surface coating, Composites Science and Technology 67 (2007) 1574–1583.
[6] R. Dangtungee, J. Yun, P. Supaphol, Melt rheology and extrudate swell of calcium carbonate nanoparticles-filled isotactic polypropylene, Polymer Test 24 (2005) 2–11.
[7] C.L. Wu, M.Q. Zhang, M.Z. Rong, K. Friedrich, Silica nanoparticles filled polypropylene: effects of particle surface treatment, matrix ductility and particle species on mechanical performance of the composites, Composites Science and Technology 65 (2005) 635–645.
[8] Y.S. Thio, A.S. Argon, R.E. Cohen, M. Weinberg, Toughneing of isotactic polypropylene with CaCO$_3$ particles, Polymer 43 (2002) 3661–3674.
[9] J. Móczó, B. Pukánszky, Polymer micro and nanocomposites: structure, interactions, properties, Journal of Industrial and Engineering Chemistry 14 (2008) 535–563.
[10] C.A. Correa, A. Razzino, E. Hage Jr., Role of maleated coupling agents on the interface adhesion of polypropylene–wood composites, Journal of Thermoplastic Composite Materials 20 (2007) 323–339.
[11] J.Z. Liang, Evaluation of dispersions of nano-CaCO$_3$ particles in polypropylene matrix based on fractal method, Composites: Part A 38 (2007) 1502–1506.
[12] B. Lauke, Determination of adhesion strength between a coated particle and polymer matrix, Composites Science and Technology 66 (2006) 3153–3160.
[13] B. Lauke, T. Shuller, Calculation of stress concentration caused by coated particle in polymer matrix to determine adhesion strength at the interface, Composites Science and Technology 62 (2002) 1965–1978.
[14] Vishu Shah, Handbook of Plastics Testing and Failure Analysis, third ed., John Wiley & sons, New Jersey, 2007.
[15] Y.-H. Zhang, B.-F. Bai, J.-Q. Li, J.-B. Chen, C.-Y. Shen, Multifractal analysis of the tensile fracture morphology of polyvinylidene chloride/glass fiber composite, Applied Surface Science 257 (2011) 2984–2989.
[16] Y.-H. Zhang, B.-F. Bai, J.-B. Chen, C.-Y. Shen, J.-Q. Li, Multifractal analysis of fracture morphology of poly(ethylene-co-vinyl acetate)/carbon black conductive composite, Applied Surface Science 256 (2010) 7151–7155.
[17] A. Carbone, G. Castelli, H.E. Stanley, Time-dependent Hurst exponent in financial time series, Physica A 344 (2004) 267–271.
[18] L. Kristoufek, Multifractal height cross-correlation analysis: a new method for analyzing long-range cross-correlations, EPL 95 (2011) 68001.
[19] E. Barrera, F. Gonzalez, E. Rodriguez, J. Alvarez-Ramirez, Correlation of optical properties with the fractal microstructure of black molybdenum coatings, Applied Surface Science 256 (2010) 1756–1763.
[20] T.-P. Chang, H.-H. Ko, F.-J. Liu, P.-H. Chen, Y.-P. Chang, Y.-H. Liang, H.-Y. Jang, T.-C. Lin, Y.-H. Chen, Fractal dimension of wind speed time series, Applied Energy 93 (2012) 742–749.
[21] E. Perez, V. Alvarez, C.J. Perez, C. Bernal, Tensile and fracture behavior of polypropylene based composites reinforced with different rigid fillers, Polymer Testing, submitted for publication.
[22] R. Hansen, Thesis, University of Buenos Aires, La Dimensión de Mendès France, Relación entre su Espectro Multifractal y el Formalismo Termodinámico, Aplicación a Sistemas tipo Hénon, Buenos Aires, Argentina, 2009, URL: http://cms.dm.uba.ar/academico/carreras/doctorado/tesishansen.pdf, (in Spanish).
[23] H. Chen, X. Sun, H. Chen, Z. Wu, B. Wang, Some problems in multifractal spectrum computation using an statistical model, New Journal of Physics 6 (2004) 84–100.
[24] M. Rosen, C. Cabeza, C. Lizarralde, Multifractal spectra in the Faraday experiment, in: Proc. 9th Exp. Chaos Conf. (ECC9), São José dos Campos, São Paulo, Brasil, May 2006, 2006.
[25] M. Piacquadio, M. Rosen, Multifractal analysis of a road-to-crisis in a Faraday experiment, xxx.lanl.gov (2008) arXiv:0804.3426v2 [math-ph].
[26] N. Francois, M. Piacquadio, M. Daraio, Multifractal analysis of scleroglucan hydrogels for drug delivery, Fractals 19 (3) (2011) 339–346, http://dx.doi.org/10.1142/S0218348X11005348.
[27] F.O. Redelico, M. Piacquadio, Fractal geometry of prior-to-crash market situations: the NASDAQ100 April 2000 crash case, Journal of Physics: Conference Series 221 (1) (2010), http://dx.doi.org/10.1088/1742-6596/221/1/012002.
[28] W.-X. Zhou, The components of empirical multifractality in financial returns, EPL 88 (2009) 28004.
[29] O. Malcai, D.A. Lidar, O. Biham, D. Avnir, Scaling range and cutoffs in empirical fractals, Physical Review E 56 (1997) 2817–2828.
[30] C. Liu, X.-L. Jiang, T. Liu, L. Zhao, W.-X. Zhou, Multifractal analysis of the fracture surfaces of foamed polypropylene/polyethylene blends, Applied Surface Science 255 (2009) 4239–4245.
[31] Z.-Q. Jiang, W.-X. Zhou, Multifractality in stock indexes: fact of fiction? Physica A 387 (2008) 3605–3614.
[32] W.-X. Zhou, Finite-size effect and the components of multifractality in financial volatility, Chaos, Solitons & Fractals 45 (2012) 147–155.